Contaminant exposure in a pharmacy cleanroom with mixing ventilation: Impact of air-change rates

Peng Qin [1,*], *Twan* Van Hooff [1], *Marcel* Loomans [1] and *Roberto* Traversari [2]

[1]Building Physics and Services, Department of the Built Environment, Eindhoven University of Technology, Eindhoven, The Netherlands
[2]Department of Buildings and Energy Systems, TNO Netherlands Organization for Applied Scientific Research, Delft, The Netherlands

Abstract. Ventilation is one of the primary strategies for controlling the contaminant exposure in a room. However, a lack of understanding in ventilation can lead to misinformation in estimating contaminant exposure. This includes the challenge of determining an appropriate ventilation flow rate (air changes per hour, ACH) and the airflow patterns required to keep aerosol particle concentrations limited. The goal of this work package of the P3Venti program is to investigate the impact of different values of ACH on the efficiency of contaminant removal in a pharmacy cleanroom employing mixing ventilation. The analysis combines experiments and CFD simulations. First, the CFD results of velocity magnitude, temperature, and particle concentration are validated with experimental data for the specific room. Next, the impact of ACH (i.e. 1.5, 3, 6, 10, 20, 40 h^{-1}) on the distributions of velocity magnitude, temperature, and particle concentration is systematically analyzed. The results show that the buoyancy effect is significant at low ACH values, whereas the mixing effect becomes dominant at high ACH values. As ACH increases, the index of concentration reduction increases from approximately 48.5% to 96.5%, with most significant effects when ACH increases from 1.5 to 10 h^{-1}. Similar follow-up research will be conducted for classrooms and general rooms in, e.g., long-term care facilities.

1 Introduction

Various studies have shown that viruses can survive in the air through aerosol particles (e.g. [1]). A comprehensive understanding of airflow patterns and ventilation rates, particularly in the presence of stationary objects within a room, is essential to achieve the objective of efficiently decontaminating spaces from particles laden with viruses. The research program Pandemic Preparedness and Ventilation (P3Venti) was initiated to develop knowledge on the role of airborne spread (aerogenic route) of viruses and other pathogens, to increase the effectiveness of using ventilation as a mitigation measure and to develop methods and tools to support government and societal partners in often complex and sensitive decision making.

Ventilation is one of the primary strategies for controlling contaminant exposure in a room. However, a lack of understanding in ventilation can lead to misinformation in estimating contaminant exposure. The goal of this part of the P3Venti program is to investigate the impact of the number of air changes per hour (ACH) and air distribution system on the efficiency of contaminant removal, here aerosols, in a pharmacy cleanroom employing mixing ventilation. The analysis combines experiments and computational fluid dynamics (CFD) simulations. First, the CFD results in terms of velocity magnitude, air temperature, and particle concentration are validated with experimental data for the specific room. Next, the impact of ACH (i.e. 1.5, 3, 6, 10, 20, 40 h^{-1}) on the velocity magnitude, temperature, and particle concentration distributions is systematically analyzed.

This paper is organized as follows. *Section 2* describes the details of the experiment conducted in a pharmacy cleanroom. *Section 3* describes the computational settings and parameters for the CFD simulations. *Section 4* presents the validation of the CFD results. *Section 5* discusses the impact of ACH, *Section 6* describes the limitations and *Section 7* closes the paper with conclusions.

2 Description of the experiment

This section describes the experiments conducted in a pharmacy cleanroom with mixing ventilation. The experiments were performed by TNO [2] but are reiterated here as the basis for the CFD validation. The experimental data in terms of velocity, temperature, and particle concentrations were used to validate the accuracy of the CFD method.

Figure 1 shows a photo of the experimental setup in the pharmacy cleanroom. This pharmacy cleanroom has dimensions of 6.4 m (length) × 3.3 m (width) × 2.8 m (height), corresponding to a volume of about 59.1 m^3. The mixing ventilation system is composed of three

* Corresponding author: p.qin@tue.nl

swirl diffusers to supply the air to the room and two outlets located at side walls to exhaust the air. The three swirl diffusers are uniformly installed at the room's ceiling level, spaced at intervals of 0.6 m from side to side. Two persons were considered in the experiments which were represented by two thermal manikins, standing face to face at each end of the table. The relative distance between the two thermal manikins was 2.30 m. For each thermal manikin, the upper body was wrapped with a heat blanket and the output power was about 80 watts. To replicate a realistic pharmacy cleanroom condition, one operation cabinet and two tables were also included in the experiment.

During the experiment, three variables were measured: velocity, temperature, and particle concentration. For velocity and temperature measurements, the ClimaCube 3D acoustic sensors (http://www.humitemp.com) were utilized. These sensors have a velocity measurement range of 0.03 m/s to 3 m/s with an accuracy of ±0.03 m/s, and a temperature measurement range of 10 ℃ to 40 ℃ with an accuracy of ±0.1 ℃. The sensors were positioned at 26 locations where velocity and temperature data were collected at 6 different heights: 0.12 m, 0.48 m, 0.82 m, 1.17 m, 1.52 m, and 1.88 m. The sampling period was set to 30 s with a data recording frequency of 0.5 Hz which provided a rough estimate of the air speeds that occur (future work will include more detailed measurements by TNO). For particle concentration measurement, one TOPAS GmbH atomizer aerosol generator ATM 228 was used to generate particles ranging from 0.5-5 µm. The particle emitter (PE) was placed on the table and close to the thermal manikin. The paraffin oil was selected as the aerosol substance and the test particles were generated by atomizing paraffin oil solutions in the aerosol generator. The nozzle pressure in the aerosol generator was kept constant at 50 hPa during the measurements. The corresponding airflow rate at the aerosol outlet surface was approximately 0.9 L/min. Six Lighthouse Handheld 3016 particle counters (PCs) were used to measure the particle concentrations. Throughout the measurement process, particle concentrations were recorded for particle sizes of 0.3, 0.5, 0.7, 1.0, 2.0, and 5.0 µm, identified as PM0.3, PM0.5, PM0.7, PM1.0, PM2.0, and PM5.0 in this study. Each particle measurement process consisted of three stages with the following durations: (*i*) baseline concentration stage for 5 minutes, (*ii*) mixing stage for 10 minutes, and (*iii*) cleaning stage for 30 minutes. The baseline concentration stage represented the background particle concentration level without the particle generator working, the mixing stage represented the mixing process of the aerosol particles by the swirl diffusers together with the particle generator working, and the cleaning stage represented the cleaning process of the aerosol particles without the particle generator working. Note that the mechanical mixing ventilation kept working during the whole process. The recording frequency for concentration was set to 0.067 Hz and sampling continued throughout the whole process.

Fig. 1. Photo of the experimental setup in the pharmacy cleanroom.

3 CFD simulations: computational settings and parameters

3.1 Computational domain and grid

Figure 2 shows the computational domain and the computational grid used for the CFD simulations. The computational domain is a replication of the aforementioned pharmacy cleanroom, with dimensions of 6.4 m × 3.3 m × 2.8 m. The three swirl diffusers, thermal manikins, the operation cabinet, and tables are explicitly modeled in the computational domain to closely reproduce the experimental setup. Note that the thermal manikins are simplified versions of those used in the experiment, and the PE is substituted with a small cylinder measuring 0.008 m in diameter and 0.01 m in height. The origin is set at the corner of the computational domain, as shown in Figure 2a. The computational grid (Fig. 2b) was determined by the grid-sensitivity analysis (GsA) using three different levels of refinement: *coarse* (about 1.9 million cells), *basic* (about 4.9 million cells) and *fine* (about 8.2 million cells). For sake of brevity, the three grids and the GsA results are not reported in this paper. The *basic* grid (Fig. 2b) is retained in this study.

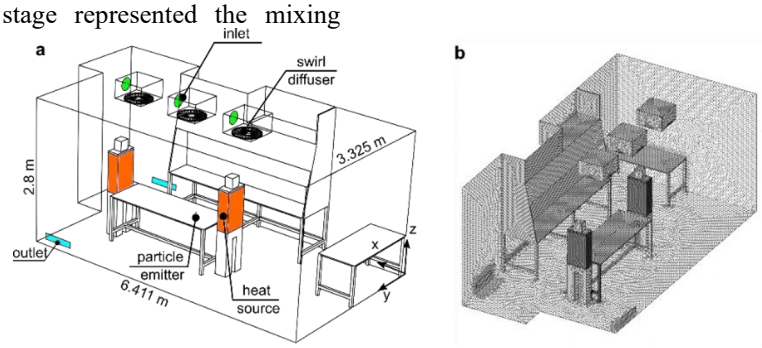

Fig. 2. (a) The computational domain and (b) the computational grid.

3.2 Boundary conditions

At the inlet faces (green in Fig. 2), mass flow inlets were imposed, each with a mass flow rate of 0.0677 kg/s, corresponding to a total ACH of 10 h^{-1} as present during the experiments. The inlet air temperature was set to 20 °C. At the outlet faces (cyan in Fig. 2), zero static gauge pressure was imposed. At the upper body of the thermal manikins (orange in Fig. 2), the surfaces were set as the heat sources as in the experiment, with a surface heat flux of 76.4 W/m^2, yielding a total of 80 Watts per manikin. At the exhaust of the PE, a uniform inlet velocity of 0.30 m/s and a hydraulic diameter of 0.008 m was imposed. In addition, for the mass fraction, a specified value of 0.0242, 0.0555, 0.0823, 0.158, 0.444, 0.236 was used for PM0.3, PM0.5, PM0.7, PM1.0, PM2.0, and PM5.0, respectively. Note that these mass fractions were obtained by averaging the measurements from each PC across all six counters. On all the other surfaces except the inlet face, the outlet face, the upper body of thermal manikins and the exhaust of PE, an adiabatic boundary condition was imposed, with an emissivity of 0.9.

3.3 Other computational settings

All the simulations were performed with Ansys Fluent 2021R1 [3]. 3D steady Reynolds-averaged Navier-Stokes (RANS) simulations were performed using the RNG k-ε turbulence model [4] with the scalable wall function. The surface-to-surface (S2S) radiation model was applied to model the radiative heat transfer. The drift flux model [5] was used to model the particle dispersion of PM0.3, PM0.5, PM0.7, PM1.0, PM2.0, and PM5.0. A total of six user-defined scalars were employed to solve the particle dispersion of PM0.3, PM0.5, PM0.7, PM1, PM2, PM5. Second-order upwind discretization schemes were used for all variables. For pressure interpolation, the staggered scheme PRESTO! was applied. Pressure-velocity coupling was solved using the pseudo-transient under-relaxation method. The incompressible ideal gas law was used for buoyancy.

4 CFD simulations: validation

Figure 3 shows the comparison of CFD and measurement results in terms of velocity magnitude (V_{mag}) along 26 vertical lines across the pharmacy cleanroom. At vertical lines 03, 06, 08, 18, 19, 20, 21, and 26, a satisfactory agreement is observed between CFD and measurement data. The CFD model effectively predicts the V_{mag} and their trends along the z-direction. However, a less satisfactory agreement is noted at vertical lines 02, 04, 05, 09, 10, 11, 14, 15, 16, 17, 24, and 25. While the trend of V_{mag} variation along the z-direction closely resembles that of the measurement results, significant disparities in V_{mag} can be observed between the CFD and measurement data. As for other vertical lines 01, 07, 12, 13, 22, 23, the CFD provides inaccurate predictions of V_{mag} values and their trends with respect to the measurement data. One possible reason might be the deficiency of the CFD approach in accurately predicting the low-velocity values in a complex indoor environment. The mean-averaged absolute difference in terms of V_{mag} between CFD and measurement and the corresponding standard deviation over the 156 measurements locations are about 0.08 m/s and 0.05 m/s, respectively.

Figure 4 shows the comparison of CFD and measurement results in terms of temperature (T_{air}) along 26 vertical lines across the pharmacy cleanroom. A satisfactory agreement in terms of T_{air} is obtained between the CFD and experiment, with the mean-averaged absolute difference being approximately 0.09 °C. However, large differences can be found at the lower level (i.e. z = 0.12 m) of the room. The exact reason for this is still unclear, however, it may be due to the fact the walls and floor were not completely adiabatic in practice.

Figure 5 displays the comparison of CFD and measurement results in terms of dimensionless particle concentration (C/C_R) at PC2, PC3, PC4, PC5 and PC6, with respect to the reference particle concentration (C_R) at PC1, for PM0.3, PM0.5, PM0.7, PM1.0, PM2.0, and PM5.0. Overall, a satisfactory agreement in terms of C/C_R is obtained between CFD and measurement data. However, it should be noted that CFD may overestimate/underestimate C/C_R to a certain extent when compared to the measurement for different locations. For instance, at PC5, CFD significantly overestimates C/C_R for PM0.3, PM0.5, PM0.7, PM1.0, PM2.0, and PM5.0. One potential reason could be the proximity of PC5 to the wall, where the CFD model may face challenges in precisely capturing the flow characteristics near the wall.

Figure 6 shows the scatter plot of CFD and experimental results for V_{mag}, T_{air} and C/C_R. In terms of V_{mag} (Fig. 6a), approximately 39% (60/156) and 76% (118/156) of the CFD-predicted values are within the 30% and 60% ranges, respectively, of the experimental velocity magnitude values. Despite the deviations in V_{mag}, it is important to note these absolute values are low (< 0.22 m/s) and the mean-averaged absolute difference between CFD and the experiment over all the measurement positions is about 0.08 m/s. In terms of T_{air} (Fig. 6b), all CFD-predicted values deviate by less than 1 °C from the experimental temperature values. In terms of C/C_R (Fig. 6c), almost all (155/156) of the CFD-predicted values are within the 40% range of the experimental C/C_R values.

Overall, the present CFD-predicted results regarding the V_{mag}, T_{air} and C/C_R show satisfactory agreement with the experimental results. For this reason, the CFD closed by the RNG turbulence model is retained for the analysis concerning the impact of ventilation air-change rates (Section 5).

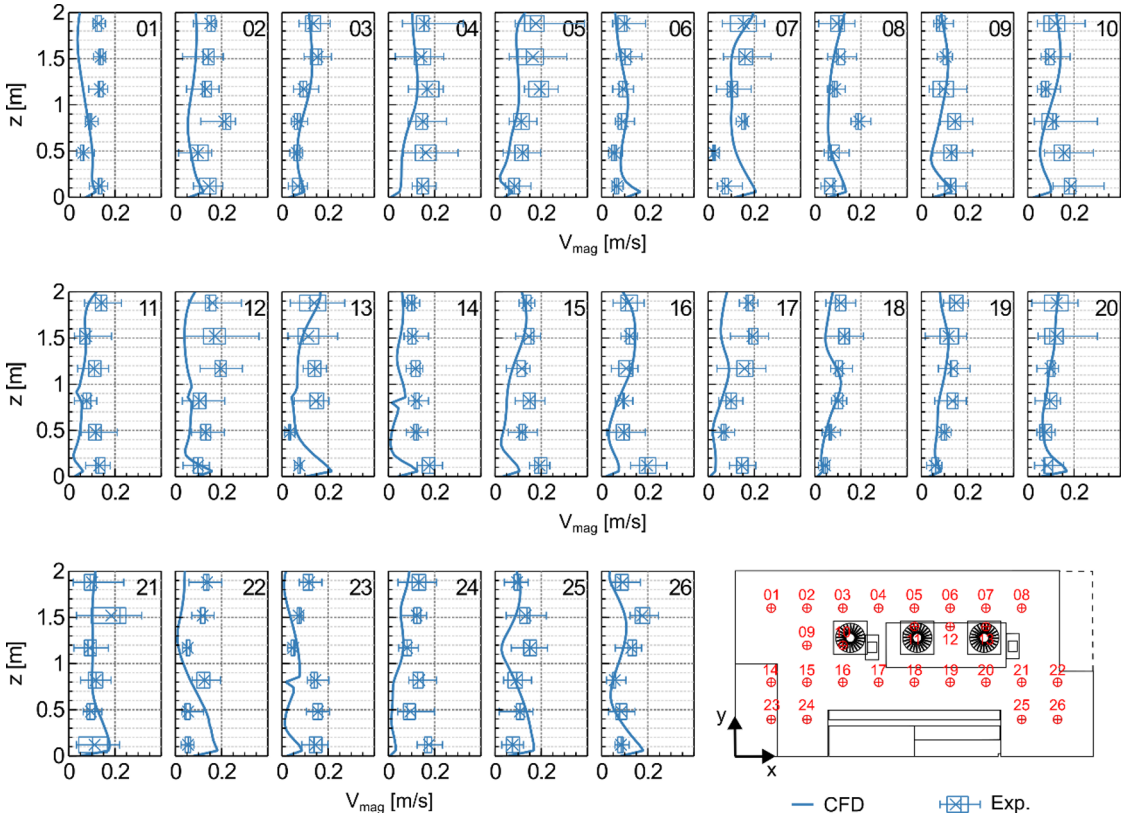

Fig. 3. Comparison of CFD and measurement results in terms of velocity magnitude (V_{mag}) along 26 vertical lines across the pharmacy cleanroom.

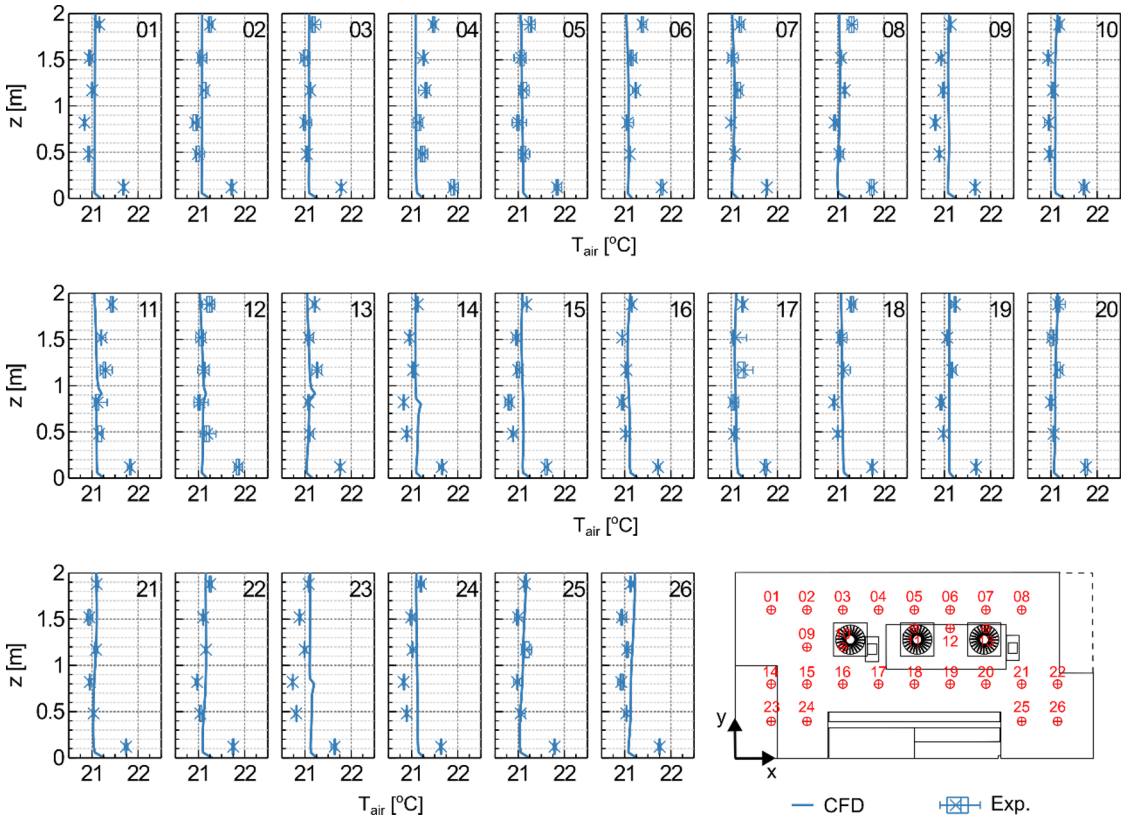

Fig. 4. Comparison of CFD and measurement results in terms of air temperature (T_{air}) along 26 vertical lines across the pharmacy cleanroom.

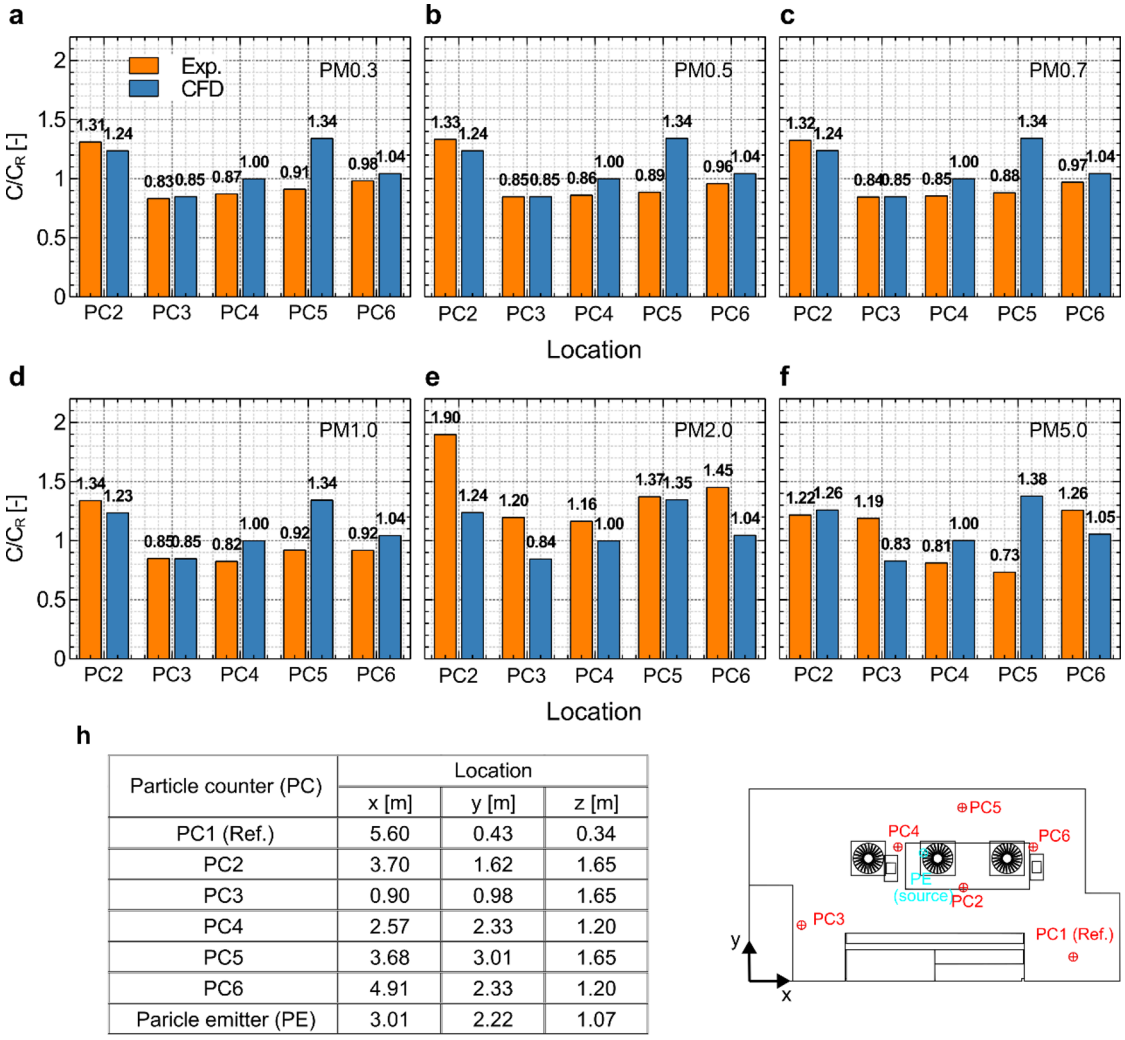

Particle counter (PC)	Location		
	x [m]	y [m]	z [m]
PC1 (Ref.)	5.60	0.43	0.34
PC2	3.70	1.62	1.65
PC3	0.90	0.98	1.65
PC4	2.57	2.33	1.20
PC5	3.68	3.01	1.65
PC6	4.91	2.33	1.20
Paricle emitter (PE)	3.01	2.22	1.07

Fig. 5. Comparison of CFD and measurement results in terms of dimensionless particle concentration (C/C_R) at PC2, PC3, PC4, PC5 and PC6, with respect to the reference particle concentration (C_R) at PC1, for (a) PM0.3, (b) PM0.5, (c) PM0.7, (d) PM1.0, (e) PM2.0, and (f) PM5.0. (h) Locations of particle emitter (PE) and particle counters (PCs).

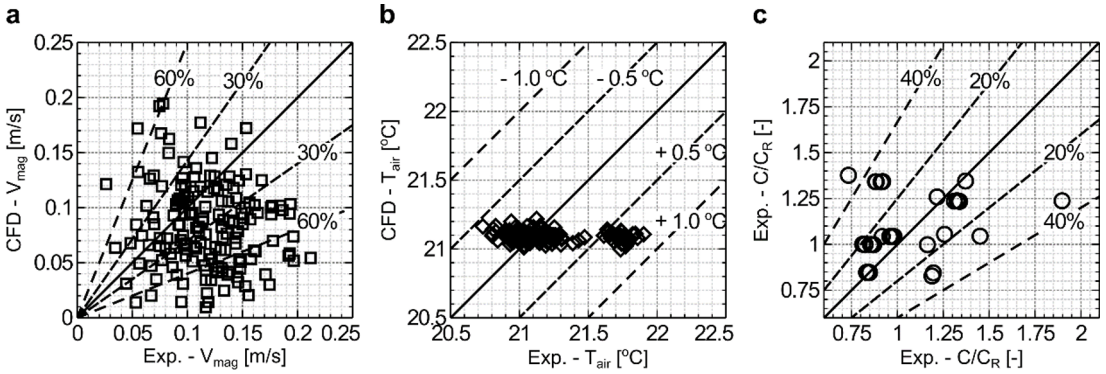

Fig. 6. Scatter plot of CFD and experimental results for (a) velocity magnitude (V_{mag}), (b) air temperature (T_{air}) and (c) C/C_R.

5 CFD simulations: Impact of ACH

This section systematically analyzes the impact of ACH (i.e. 1.5, 3, 6, 10, 20, 40 h^{-1}) on the velocity magnitude, temperature, and particle concentration distributions in the modelled pharmacy cleanroom.

Figure 7 shows the contours of V_{mag} and streamlines on a vertical plane at y = 2 m for ACH equal to 1.5, 3, 6, 10, 20, 40 h^{-1}. At low ACHs (e.g. ACH = 1.5, 3, 6 h^{-1}, Fig. 7a-c), buoyancy effects (thermal plumes) are pronounced, with a V_{mag} of about 0.2 m/s found close to the manikins. This is particular evident for the region above the left manikin (at $x \approx 5$ m), where the streamlines go upward to the ceiling. With the increase of ACH (Fig. 7d-f), the overall velocities increase in these entire vertical sections, as well as in the breathing zones above the table and between the manikins. In addition, the flow regime (i.e. streamlines) gradually stabilizes, suggesting the enhanced mixing effect at a higher ACH value (e.g. 20 h^{-1}), consequently leading to

a relative diminishment of the buoyancy effects near the manikins. At high ACH values (e.g., 10, 20, 40 h^{-1}), the flow pattern remains the same (flow similarity) with velocity magnitudes increasing, corresponding to the increment in ACH.

Figure 8 shows the contours of T_{air} on the same vertical plane (y = 2 m) for ACH equal to 1.5, 3, 6, 10, 20, and 40 h^{-1}. When a low ACH (e.g. 1.5 h^{-1}) is applied to the room, relatively high-temperature values (~24-27 ℃) are observed throughout the room, with the highest T_{air} located close to the thermal manikin. With the increase of ACH, the enhanced mixing begins to ameliorate the thermal environment by reducing T_{air} values across the room, although relatively elevated temperature values persist in the vicinity of the thermal manikin. In addition, a more uniform temperature distribution is observed at high ACH (e.g. 10, 20, 40 h^{-1}). Note that thermal comfort is not discussed in this study.

Figure 9 displays only the contours of C/C_0 for PM0.3 at a vertical plane y = 2 m, with ACH values of 1.5, 3, 6, 10, 20, and 40 h^{-1}. Similar C/C_0 distributions are observed for PM0.3, PM0.5, PM0.7, PM1, PM2, and PM5 under the same ACH value. Note that the concentration at the inlet face of the PE (i.e. C_0) is taken as the reference concentration to better estimate the impact of ACH. At low ACHs (e.g. 1.5 h^{-1}, Fig. 9a), an extensive region of high C/C_0 values (e.g. > 4.0×10^{-4}) is observed on the plane y =2 m. With an increase in ACH from 3 to 10 h^{-1} (Fig. 9b-d), a gradual decrease in C/C_0 values is observed for regions away from the source. However, the hotspot of high C/C_0 values remains pronounced near the source location for ACH = 3, 6, and 10 h^{-1}. Further increase in ACH from 20 to 40 h^{-1} (Fig. 9e-f) leads to a more uniform C/C_0 distribution with generally lower C/C_0 values (e.g. 2.0×10^{-5}) compared to ACH = 1.5, 3, 6, and 10 h^{-1}.

Two indices, namely the normalized volume-averaged concentration (C_{avg}/C_0) and the concentration reduction (C_R), are employed to quantify and estimate the impact of ACH on indoor containment exposure and removal effectiveness. The C_{avg} and C_R are calculated using Equations 1, 2:

$$C_{avg} = \frac{\int_V CdV}{V} \quad (1)$$

$$C_R = \frac{C_{avg}^{ACH=1.5h^{-1}} - C_{avg}^{ACH=ih^{-1}}}{C_{avg}^{ACH=1.5h^{-1}}} \quad (2)$$

where V is the volume of the specific room, and $C_{avg}^{ACH=1.5h^{-1}}$ is the C_{avg} at ACH = 1.5 h^{-1}, serving as the reference for C_R calculation. The C_{avg}/C_0 and C_R curves as a function of ACH for PM0.5, PM0.7, PM1.0, and PM2.0 almost overlap with those for PM0.3. For the sake of brevity, Figure 10 displays only the impact of ACH on C_{avg}/C_0 and C_R for PM0.3 and PM5.0. In terms of C_{avg}/C_0 (Fig. 10a), at ACH = 1.5 h^{-1}, a higher value is found for PM0.3 (5.28) with respect to PM5.0 (3.42). This could be attributed to the increased deposition of PM5.0 at low ACH, especially when compared to particles of smaller sizes (e.g. PM0.3, PM0.5, PM0.7, PM1.0, and PM2.0). With an increase in ACH, the deviation of C_{avg}/C_0 between PM0.3 and PM5.0 diminishes, which is barely discernible after ACH = 10 h^{-1}. Additionally, it is observed that the value of C_{avg}/C_0 for PM0.3 and PM5.0 decreases with the increase in ACH. Overall, the increase in ACH reduces the contaminant exposure in this specific room. In terms of C_R (Fig. 10b), as ACH increases from 1.5 h^{-1} to 10 h^{-1}, a sharp rise in C_R is observed, reaching approximately 84.5% and 77.6% for PM0.3 and PM5.0, respectively. As ACH continues to increase from 10 h^{-1} to 20 h^{-1}, a gradually slower increase in C_R is observed, resulting in C_R of approximately 92.3% and 89.1% for PM0.3 and PM5.0, respectively. After ACH reaches 20 h^{-1}, an approximately flat trend is observed, indicating that the effect of additional ventilation decreases, as to be expected. The C_R at ACH = 40 h^{-1} is about 96.5% for PM 0.3 and 93.8% for PM5.0, respectively.

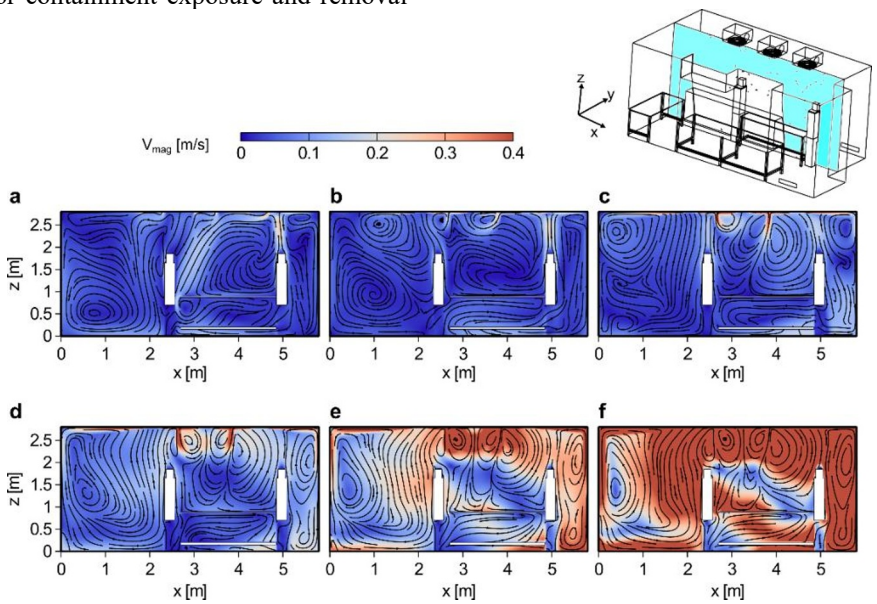

Fig. 7. Contours of the velocity magnitude and streamlines on a vertical plane at y = 2 m for ACH equal to (a) 1.5 h^{-1}, (b) 3 h^{-1}, (c) 6 h^{-1}, (d) 10 h^{-1}, (e) 20 h^{-1}, (f) 40 h^{-1}.

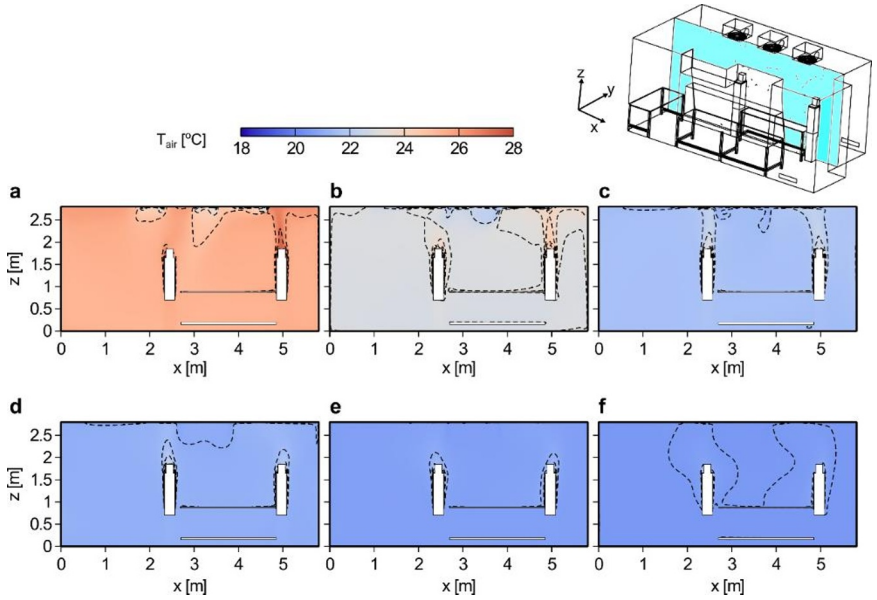

Fig. 8. Contours of the temperature on a vertical plane y = 2 m for ACH equal to (a) 1.5 h^{-1}, (b) 3 h^{-1}, (c) 6 h^{-1}, (d) 10 h^{-1}, (e) 20 h^{-1}, (f) 40 h^{-1}.

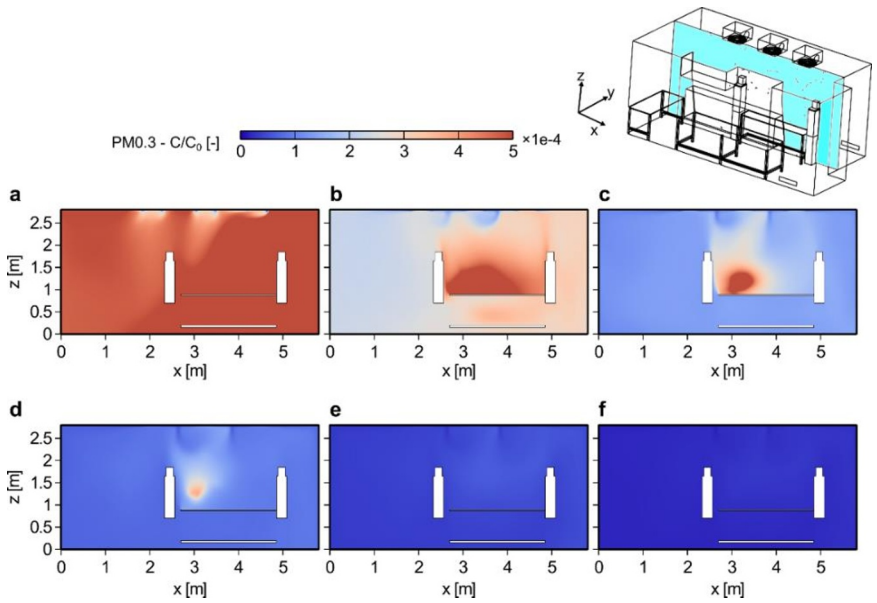

Fig. 9. Contours of C/C_0 for PM0.3 on a vertical plane at y = 2 m for ACH equal to (a) 1.5 h^{-1}, (b) 3 h^{-1}, (c) 6 h^{-1}, (d) 10 h^{-1}, (e) 20 h^{-1}, (f) 40 h^{-1}.

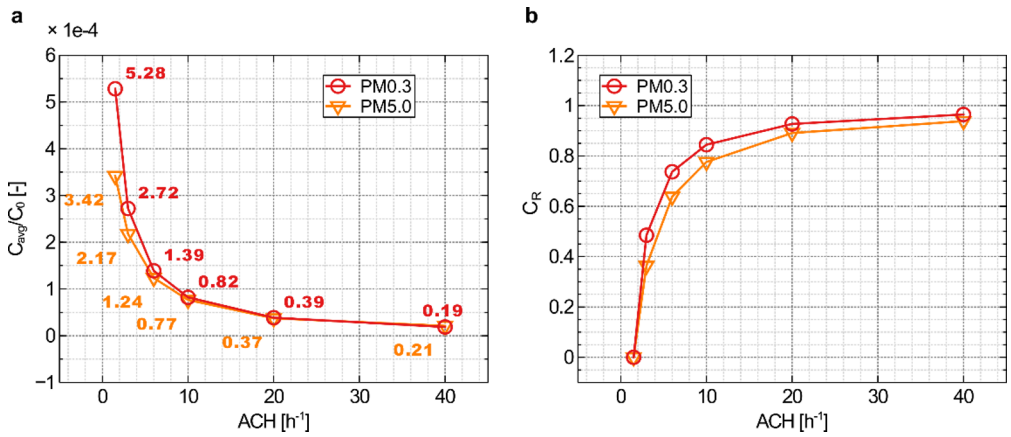

Fig. 10. Impact of ventilation air-change rate (ACH) on (a) the normalized volume-averaged concentration (C_{avg}/C_0) and (b) the concentration reduction (C_R) for PM0.3 and PM5.0.

6 Limitations

Some limitations of the present study are:

- Only a limited number of velocity samples are recorded to obtain the mean V_{mag}.
- In the present CFD simulations, adiabatic walls are assumed, while in practice the walls and floor may not be entirely adiabatic.
- Particulate matter is released from table height at a constant rate. However, for a more comprehensive assessment of airborne infectious pathogen spread, considering realistic respiratory activities like breathing, coughing, or sneezing from manikins is worth contemplating.

7 Conclusions

This study is part of the P3Venti program and aims to investigate the impact of different ACH values on the efficiency with which contamination, here aerosols, in a pharmacy cleanroom with mixing ventilation, can be removed. 3D steady RANS simulations with the RNG k-ε turbulence model were performed to assess the impact of ACH values. First, the CFD results of velocity magnitude, temperature, and particle concentration were validated with experimental data retrieved from TNO. Next, the impact of ACH (i.e. 1.5, 3, 6, 10, 20, 40 h^{-1}) on the velocity magnitude, temperature, and particle concentration distributions was systematically analyzed. The main conclusions are as follows:

- A satisfactory agreement is observed between the CFD and experimental results in terms of velocity magnitude, air temperature, and dimensionless concentration (C/C_R). The mean averaged absolute differences in terms of velocity magnitude and air temperature between CFD and experiment over the 156 measurement locations are about 0.08 m/s and 0.09 °C, respectively. Concerning C/C_R, nearly all (155/156) of the CFD-predicted values fall within the 40% range of the experimental C/C_R values.
- At low ACHs (e.g. ACH = 1.5, 3, 6 h^{-1}), buoyancy effects (thermal plumes) are pronounced. High temperature and concentration values are found close to the thermal manikin and the source location, respectively. Conversely, at high ACH (e.g. ACH = 10, 20, 40 h^{-1}), the flow regime shifts and gradually stabilizes. Mixing becomes dominant, consequently leading to a reduction of the buoyancy effects. The results show the effect of ACH on the flow pattern development.
- The increase in ACH reduces the volume-average contaminant exposure in this pharmacy cleanroom. With increasing ACH, the concentration reduction index (C_R) rises sharply up to 84.5% (PM0.3) and 77.6% (PM5.0) at 10 h^{-1}, followed by a slower increase up to approximately 92.3% (PM0.3) and 89.1% (PM5.0) at 20 h^{-1}. However, beyond 20 h^{-1} further increases in ACH may not significantly reduce C_R, with values approximately 96.5% for PM0.3 and 93.8% for PM5.0 at ACH = 40 h^{-1}.

Acknowledgement

This research received funding from the Pandemic Preparedness Programme and Ventilation (P3Venti Program) coordinated by the Netherlands Organization for Applied Scientific Research TNO and funded by the Dutch Ministry of Health, Welfare and Sport. The authors also gratefully acknowledge the partnership with Ansys. This work was carried out on the Dutch national e-infrastructure with the support of SURF Cooperative (EINF- 2046).

References

1. P.J. Bueno de Mesquita, W.W. Delp, W.R. Chan, W.P. Bahnfleth, B.C. Singer. Control of airborne infectious disease in buildings: Evidence and research priorities. Indoor Air 32, e12965 (2022)
2. A. de Lange. MST - ENSCHEDE Meetresultaten Programmalijn III (2023)
3. Ansys Inc. ANSYS Fluent -Theory Guide 2020R1 (2020)
4. V. Yakhot, S.A. Orszag, S. Thangam, T.B. Gatski, C.G. Speziale. Development of turbulence models for shear flows by a double expansion technique. Phys. Fluids 4, 1510-1520 (1992)
5. F. Chen, S.C.M. Yu, A.C.K. Lai. Modeling particle distribution and deposition in indoor environments with a new drift-flux model. Atmos. Environ. 40, 357-367 (2006)